A BALLOON OBSERVATION OF AURORAL X-RAY IMAGES IN THE NORTHERN AURORAL ZONE

Yo Hirasima[1], Hiroyuki Murakami[1], Atsushi Nakamoto[1],
Kiyoaki Okudaira[1], Hiromu Suzuki[1], Takamasa Yamagami[2],
Shigeo Ohta[2], Michiyoshi Namiki[2], Jun Nishimura[2],
Hiroshi Miyaoka[3], Natsuo Sato[3],
Ryoichi Fujii[3] and Masahiro Kodama[4]

[1] *Department of Physics, Rikkyo University, 34–1, Nishi-
ikebukuro 3-chome, Toshima-ku, Tokyo 171*
[2] *The Institute of Space and Astronautical Science, 6–1,
Komaba 4-chome, Meguro-ku, Tokyo 153*
[3] *National Institute of Polar Research, 9–10, Kaga 1-chome,
Itabashi-ku, Tokyo 173*
[4] *Department of Physics, Yamanashi Medical College,
Tamaho, Nakakoma, Yamanashi 409–38*

Abstract: A balloon observation of auroral X-rays has been carried out by using two kinds of X-ray imagers, *i.e.*, a newly developed imager with 5×5 matrix array of Si(Li) semiconductor detectors (SSD's) and another one with one-dimensional array of 8 NaI(Tl) scintillation counters. Each of these two imagers has a pinhole collimator, which gives a resolution angle of $15°$ at the central detector (counter). The lower limits of X-ray energy measurable are 37 and 22 keV for the SSD and NaI(Tl) imagers, respectively. The balloon carrying these imagers was launched from Abelver, Norway at 2117 UT on July 5, 1985 and was flown toward Iceland. An enhancement of auroral X-ray flux was observed in the location of $L=5.2$ at ~ 2334 MLT near the geomagnetic midnight, during a geomagnetic substorm. Temporal variation of two-dimensional auroral X-ray images was derived with 3 s time resolution from SSD imager data. Also, another imager of NaI(Tl) counters confirmed the SSD results. It is shown that a sequence of auroral X-ray images obtained by two imagers are not like a stable arc structure but a localized structure with a rapid time variation. The present results suggest that localized intermittent precipitations of energetic electrons with several tens keV or greater are possible.

1. Introduction

Energetic precipitating electrons with the order of 10 keV are responsible for auroral X-rays and they are accelerated only partly in the field-aligned electric fields near the earth, but mainly in a deep magnetosphere. Thus auroral X-ray phenomena are in contrast with optical aurorae in which lower energy particles generated owing to the field-aligned acceleration are dominant.

Numerous observations of energy spectra and time variations of auroral X-rays were performed so far by a number of investigators. Also latitudinal and longitudinal movements of energetic particle precipitation regions were examined by a method of

simultaneous multiple balloons (KREMSER *et al.*, 1973, 1982; MARAL *et al.*, 1973). Although several observations of auroral X-ray spatial distributions were made, most of them were based on the sky-scanning method of using single or multiple directional X-ray counters (KODAMA and OGUTI, 1976; GOLDBERG *et al.*, 1982; HIRASIMA *et al.*, 1983; IMHOF *et al.*, 1985a). A technique of the so-called one-shot X-ray camera which should be most useful for reliable determination of spatital structure of energetic particle precipitation region is still in its initial stage of development. Two-dimensional X-ray images taken at a moment are of most importance for separation of spatial characteristics of an image from its temporal one.

MAUK *et al.* (1981) observed auroral X-ray images at a balloon altitude during a substorm, using a pinhole camera type of a scintillator X-ray imager. They found a small-scaled (~ 15 km) spatial structure of X-ray images with time resolution of 10 s, but its absolute orientation was not decided. GOLDBERG *et al.* (1982) obtained fine mapping of auroral X-rays, using a rocket-borne NaI(Tl) scintillation counter with field of view of $5°$. ULLALAND *et al.* (1984) observed an auroral X-ray source region by using an X-ray imager with 7 collimated scintillation detectors and discussed its movement. IMHOF *et al.* (1985b) observed auroral X-ray images of an isolated patch structure by using a satellite-borne proportional counter X-ray imager. They found out that the patch has a typical size of 100–300 km. Occurrences of such patch structure were frequent at higher geomagnetic activities in the night side sector. Their X-ray imager was sensitive to energies of 4–40 keV.

In the present balloon experiment, we observed auroral X-ray images with energies of 37–200 keV by a two-dimensional array of newly developed Si(Li) semiconductor detectors. Also a one-dimensional array of 8 NaI(Tl) scintillation counters sensitive to X-rays with energies of greater than 22 keV were used for cross-check observation. As a result, auroral X-ray source regions as small as 10 km were observed successively with time resolution of 3 s and they showed a rapid temporal variation.

2. Instrumentation

Two kinds of auroral X-ray imagers were used in this balloon observation. One is a one-dimensional array of 8 NaI(Tl) scintillation counters arranged on the horizontal plane. They were contained in a collimator box which was constructed by a sandwich plate of 1 mm lead and 2 mm tin in thickness and had a pinhole of 2 cm in diameter on the top side. Each of the counters is 1.5 inch in diameter and 3 mm in thickness. Mutual spacings between the adjacent counters are 22 mm each. Fields of view of the counters are $15°$ and $10°$ for the central counter and the edge, respectively. These opening angles are equivalent to the horizontal distance of 18 km, if the source layer of auroral X-rays is assumed as 100 km in height. The full field of view covered by this imager is $95°$, which corresponds to the horizontal distance of 146 km. The energy range measured is above 22 keV.

Another imager is a two-dimensional array of the lithium-drifted silicon Si(Li) semiconductor detectors (called SSD's hereafter), which was newly developed to observe hard X-rays with better space and time resolutions. The imager consists of 25 pieces of the SSD's and each of them has an effective area of 18 mm × 18 mm and the

thickness of 5 mm. They were aligned on the horizontal two-dimensional array of
5×5 pixels, where mutual spacings between the ajacent pixcels were 7 mm each. The
collimator box was quite the same type as that used for the NaI(Tl) imager. Fields of
view of the SSD's are 15° and 13° for the central one and the edge, respectively, being
equivalent to the horizontal distance of 18 km. The full field of view is 62°, or 81 km
equivalent. The SSD and preamplifier assemblies were contained in an aluminium
air-tighted chamber with a plastic plate on the top side. The inner pressure of the
chamber was kept in 1 atm to prevent any electric noise and also to make cooling of the
SSD's easy. It is essential to cool the SSD as low as 5°C or less, in which the thermal
noise of the SSD becomes so lower that measurements of X-rays with energies of 37
keV or greater are possible. In fact, a heat pipe exposed to ambient low temperature
atmosphere around the gondola was used for cooling the SSD's. Details of the SSD
imager are described elsewhere (NAKAMOTO *et al.*, 1985).

Data aquisition and processing for the two imagers and house keeping instru-
ments were performed every 1/8 s by means of the PCM telemetry system. The top-
view arrangement of these two imagers in the gondola is shown in Fig. 1. The azi-
muthal direction of the gondola was determined by a geomagnetic aspectmeter (GA)
based on the Hall effect device.
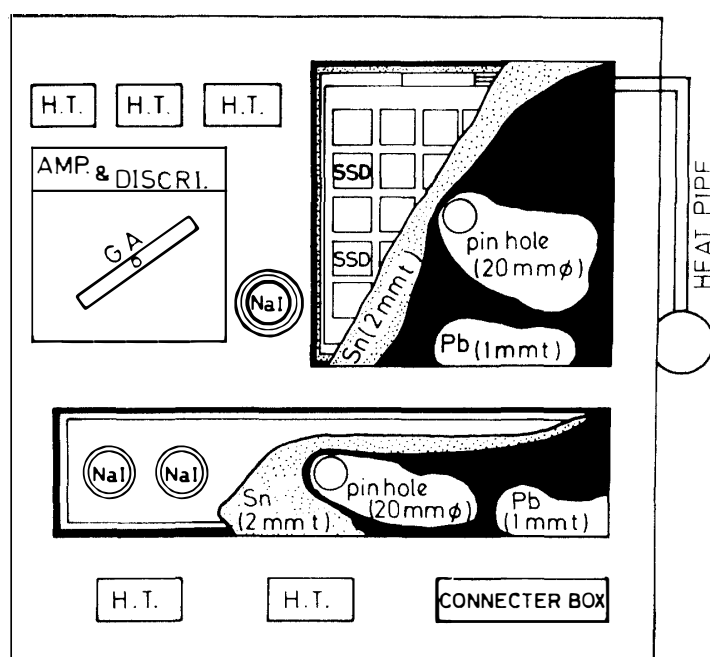
Fig. 1.   Top-view of configuration of auroral X-ray imagers.   The two-dimensional Si(Li) semi-
conductor detector (SSD) imager has 5×5 pixels.   The NaI (Tl) imager has 8 NaI(Tl)
scintillation counters.

3.   Observations

3.1.   Balloon flight and geomagnetic activity

A balloon carrying two kinds of auroral X-ray imagers was launched from Abelver

(64.7°N, 11.2°E), Norway at 2117 UT on July 5, 1985. The balloon flew westward and passed over Iceland. Telemetry signal was initially received at Abelver and later at Husavik, Iceland, until when it faded out near the location of 62.0°N and 27.2°W apart west from Iceland. The ceiling altitude of the balloon was 9 mb. An increase of auroral X-ray was observed at ~2330 UT on July 6, when the balloon was
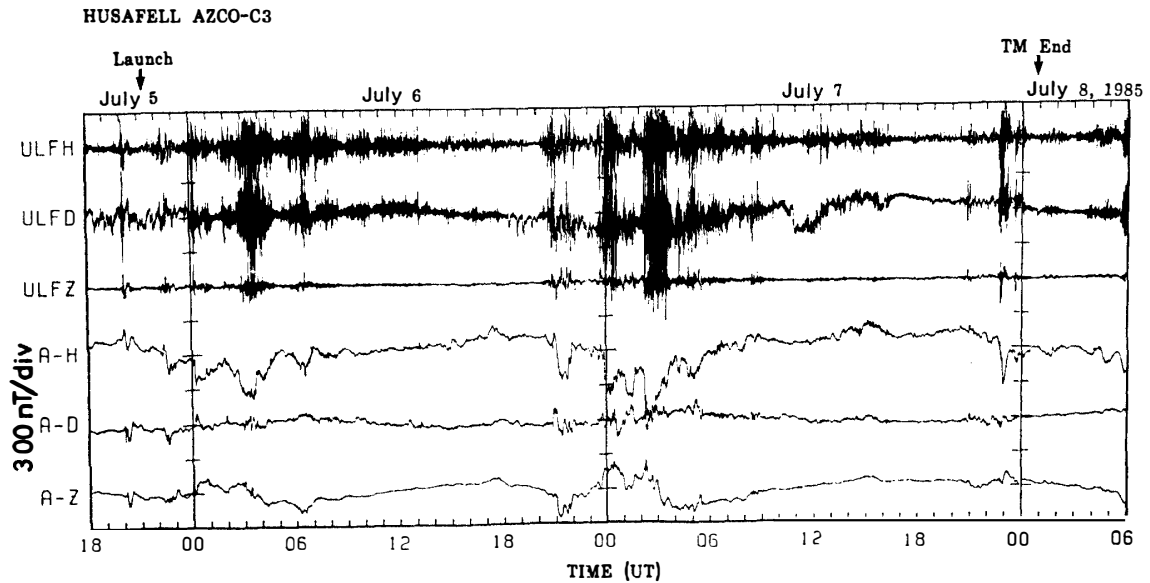
Fig. 2. ULF (0.01–5 Hz) data and magnetogram at Husafell, Iceland.
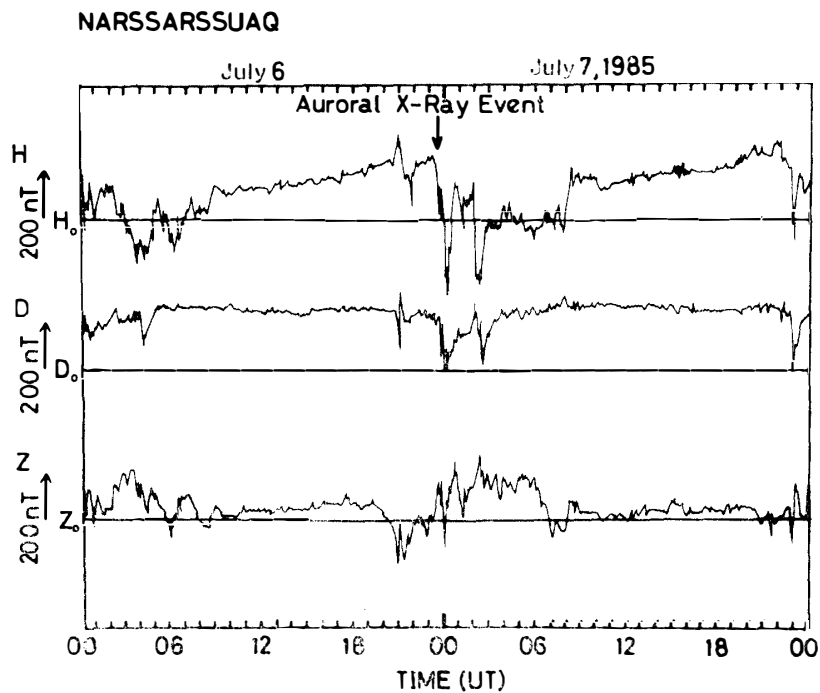
Fig. 3. Magnetogram at Narssarssuaq, Greenland. The auroral X-ray increase event in the present work is shown with an arrow.

located at 64.5°N, 7.7°W ($L=5.2$), about 250 km east from Iceland. At that time, a geomagnetic substorm was in progress, as seen from the magnetogram and ULF (0.01–5 Hz) records obtained at Husafell (64.7°N, 21.0°W; $L=6.0$), Iceland (Fig. 2), and another magnetogram at Narssarssuaq (61.2°N, 45.4°W; $L=6.7$), Greenland (Fig. 3). The substorm was a successive multiple-onset type. The geomagnetic horizontal components at these two stations varied as much as ~ 1000 nT. The first substorm started at 2100 UT on July 6, and a large negative bay occurred at 2330 UT on July 6. The planetary 3-hourly index at 2100–2400 UT was found to be 5. Thus it is evident that this auroral X-ray increase event occurred during an active substorm.

3.2. Auroral X-ray images

Temperatures of the individual Si(Li) detectors of the SSD imager were kept in $0°C \sim +6°C$ throughout the entire level flight. Noise levels of 7 SSD's were rather high even at this temperature range, but noises of the remained 18 SSD's were low enough to detect any significant enhancement of X-rays. As the SSD imager rotated azimuthally, the correct counting rates of the above noisy SSD's could be interpolated from those of the neighboring SSD's in the adjacent time interval. Some examples of time profiles of X-ray counting rates obtained by the SSD's are shown in Fig. 4, where the time interval from 2325:30 to 2345:50 UT on July 6 is selected. The SSD number attached in the figure stands for the position in 5×5 matrix. Differences among the respective time profiles of X-ray counting rates indicate a possible temporal variation of auroral X-ray images.

Corresponding time profiles obtained by the NaI(Tl) imager are shown in Fig. 5. The counting rates increased similarily at ~ 2330 UT. Since the pinhole of the collimator was located just in the center of 8 NaI(Tl) counters array, an half of the gondola rotation was enough to scan the whole sky. Therefore, one picture of auroral X-ray image could be obtained every half rotation.

The sequential auroral X-ray images obtained by the SSD imager are shown in Fig. 6, with the successive matrix maps of the counting rates. One matrix map is made up by using 3 s counting rates and one grade among small shaded squares corresponds to 3σ count, where σ ($\sigma = \sqrt{B}$) is the standard deviation of background counts B. If a counting rate is high enough, a position of an X-ray image being seen by a regular square pixel is determined longitudinally or transversely with accuracy of $1/\sqrt{6}$ times the side-length of pixel (see Appendix). The auroral X-ray counting rate maps of Fig. 6 were obtained every 3 s, while the SSD imager rotated azimuthally with ~ 1 rpm. So, the SSD imager rotated azimuthally by $\sim 20°$ during 3 s. As a result, a specified auroral X-ray source region was observed by the neighboring pixel detectors looking at with successive overlapping field of view. Two-dimensional auroral X-ray images derived from the SSD counting rates are shown in Fig. 7, where top-views of the X-ray images are illustrated. One grade of shaded area corresponds to 3σ. As shown in Fig. 7, auroral X-ray source regions were not fixed but changed with time. These results suggest that auroral X-ray sources in this event showed both time variations and irregular spatial structure, *i.e.*, several localized excess count regions of auroral X-ray flux varying rapidly with time.

Next, the auroral X-ray images obtained from the NaI(Tl) imager are presented.
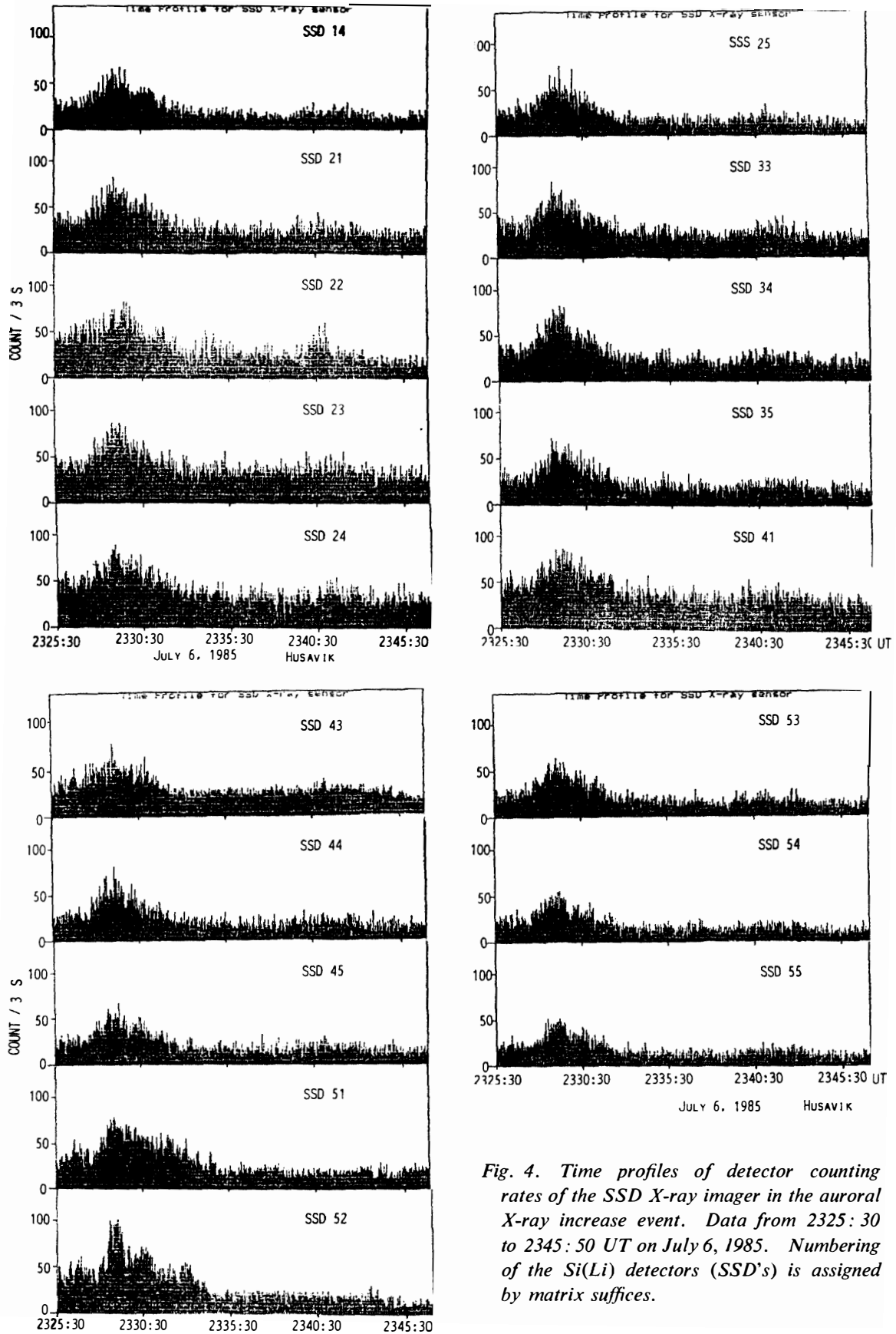
Fig. 4. Time profiles of detector counting rates of the SSD X-ray imager in the auroral X-ray increase event. Data from 2325:30 to 2345:50 UT on July 6, 1985. Numbering of the Si(Li) detectors (SSD's) is assigned by matrix suffices.
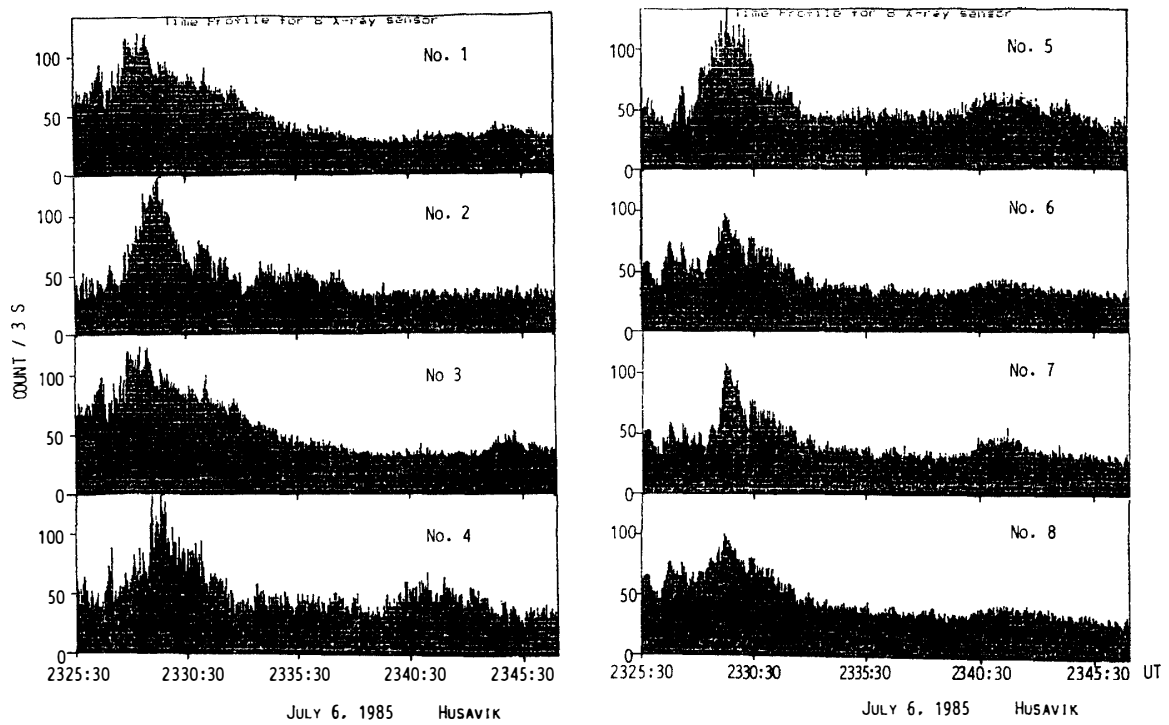
Fig. 5.   Time profiles of counting rates of 8 NaI(Tl) scintillation counters.   Data from 2325 : 30 to
         2345 : 50 UT on Junly 6, 1985.
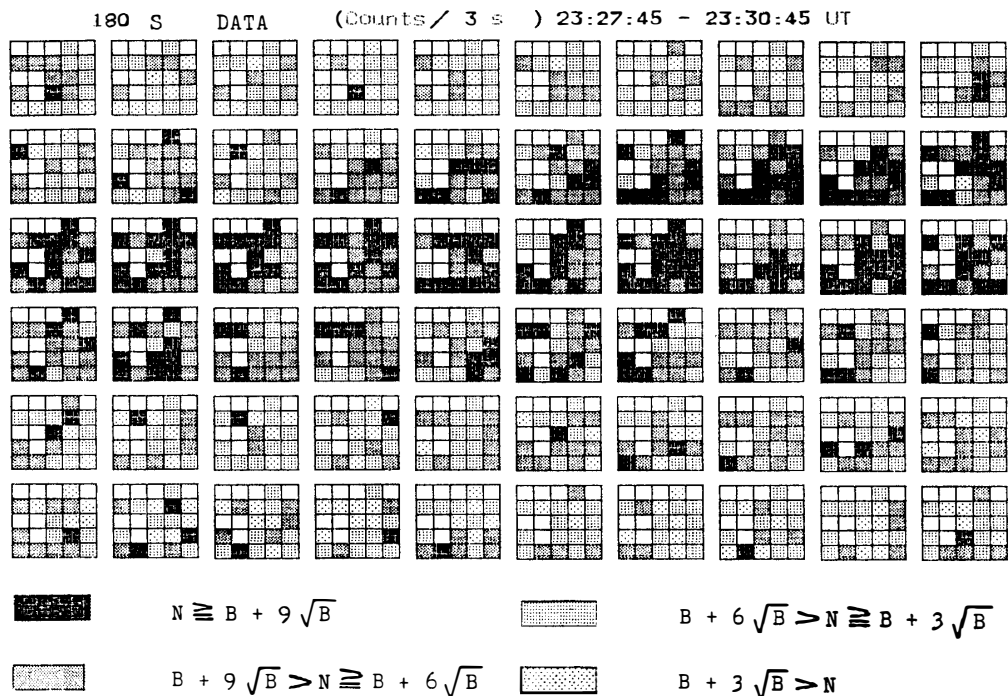
Fig. 6.   Sequential presentation of matrix maps of SSD counting rates (N).   Each map corresponds
         to count accumulation for 3 s.   One grade of shade difference corresponds to 3σ count in-
         crease or decrease ($\sigma = \sqrt{B}$: the standard deviation equivalent to fluctuation of background
         counts (B)).   Sequential times progress from left to right in each line of maps, and the lines
         are from top to bottom with time.

23:27:42-23:27:45 23:28:15-23:28:18 23:28:33-23:28:36 23:28:51-23:28:54 23:29:06-23:29:09

8 1 km

23:29:21-23:29:24 23:29:39-23:29:42 23:29:54-23:29:57 23:30:06-23:30:09 23:30:27-23:30:30

23:30:45-23:30:48 23:31:48-23:31:51 23:32:33-23:32:36 23:33:18-23:33:21

N_m

E_m
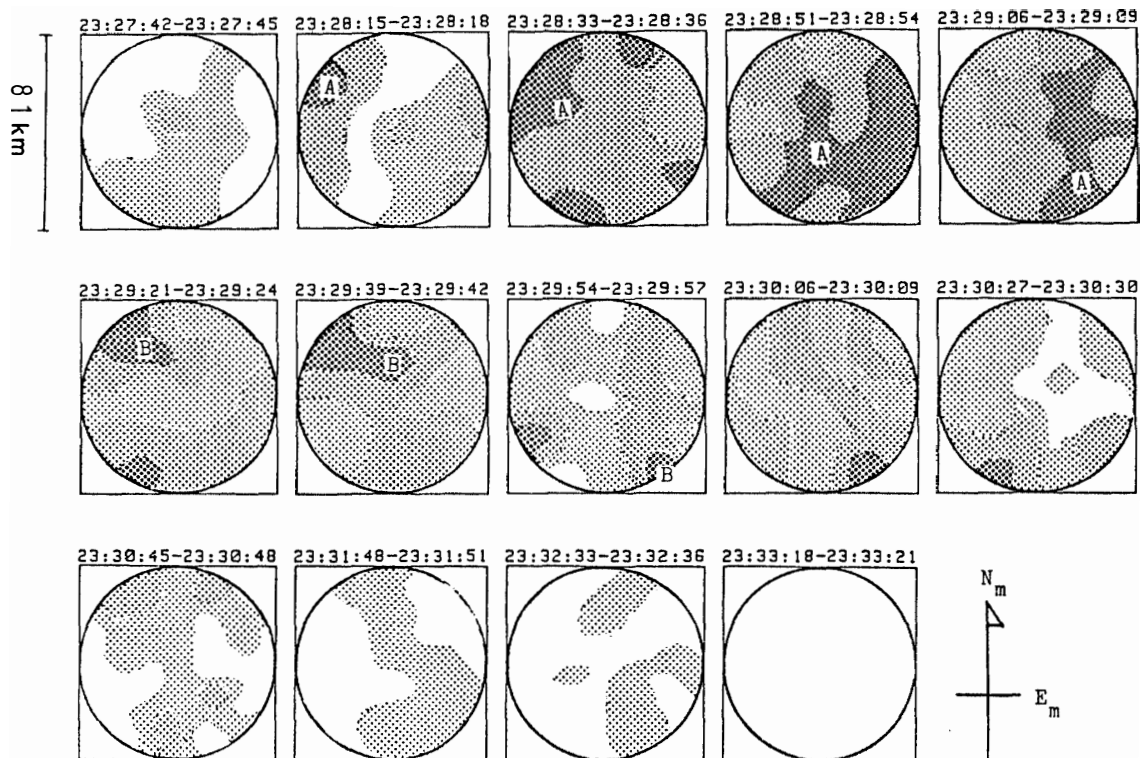
Fig. 7. *Two-dimensional auroral X-ray images derived from the data of the Si(Li) detector (SSD) imager. The figure is top-view. The darkest parts in the figure are the most bright X-ray source regions. Direction of N_m shows the geomagnetic northward. X-ray images have no simple stable arc structure. Bright regions labeled as A and B (in seven images during 2328: 15–2329: 57 UT) drifted slowly with ~50 km min^{-1} (with some uncertainty) roughly to the geomagnetic south-east.*

Successive patterns of 3 s counting rates obtained during the same event are shown in Fig. 8, where the grade representation is the same as in Fig. 6. Similarly, one picture of auroral X-ray image was obtained every half rotation and then successive patterns of that are shown in Fig. 9 (note that time intervals are different from picture to picture because of non-uniform rotation). Separation between spatial and temporal variation were not enough in this case, because ~30 s was necessary to obtain an X-ray image.

Figure 9 shows the auroral X-ray images being a little different from that of Fig. 7. This is due to the fact that the time interval necessary for composing an image is longer than in the SSD imager and also due to the difference in the lower limit of X-ray energy detectable between the two detectors. However, a similar gross feature is recognized between the both images. It is evident from Figs. 7 and 9 that a number of localized source regions appeared or disappeared with time. Furthermore, systematic spatial drifts of some source regions were observed, for example, two bright regions, labeled "A" and "B", showed similar movements roughly toward the geomagnetic south-east, with a slow velocity of about 50 km min^{-1}.

360 S   DATA   (Counts／ 3 s) 23:26: 0 – 23:32:00 UT

Legend:

$N \geqq B + 12 \sqrt{B}$

$B + 12 \sqrt{B} > N \geqq B + 9 \sqrt{B}$

$B + 9 \sqrt{B} > N \geqq B + 6 \sqrt{B}$

$B + 6 \sqrt{B} > N \geqq B + 3 \sqrt{B}$

$B + 3 \sqrt{B} > N$
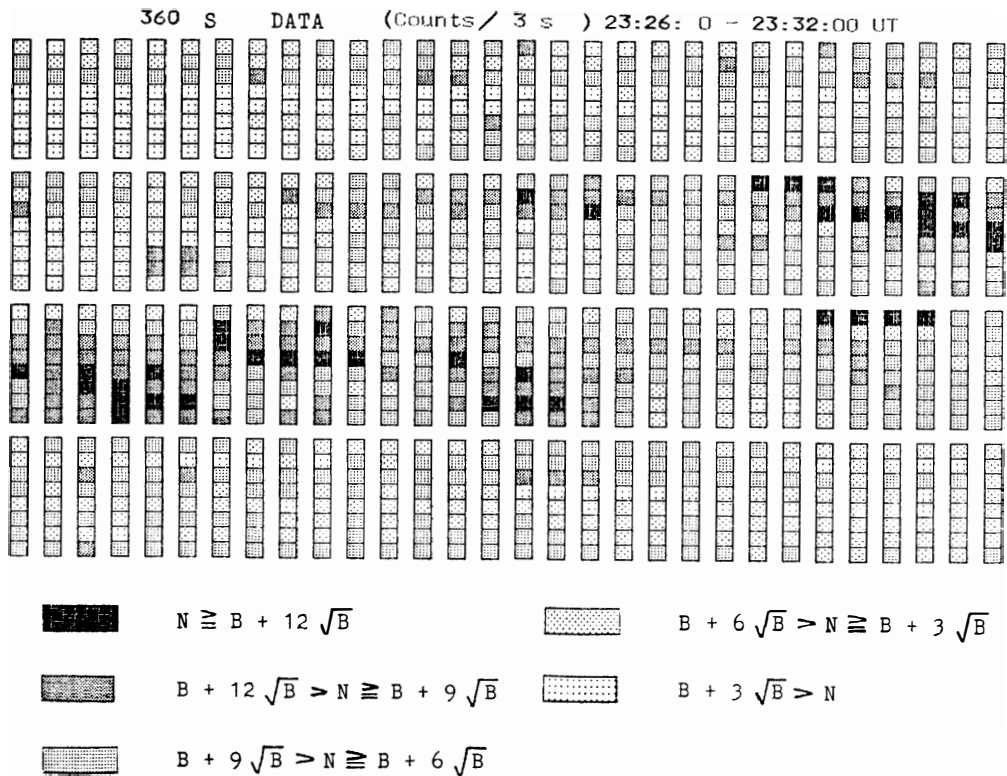
Fig. 8. Sequential presentation of counting rates (N) of the 8 NaI(Tl) counters. Each vertical train of counting rates is accumulated for 3 s. One grade of shade difference corresponds to 3σ ($\sigma = \sqrt{B}$) count increase or decrease. Sequential times progress from left to right in each of 4 lines of maps. Top line shows the change in the first 90 s.

23:27:45–23:28:36   23:28:36–23:29:09   23:29:09–23:29:34

23:29:34–23:30:09   23:30:09–23:30:48   23:30:48–23:31:51
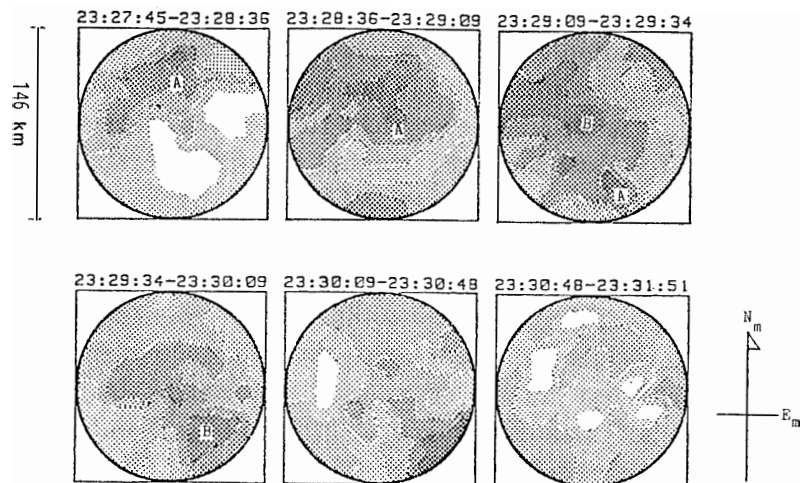
Fig. 9. Top-views of the auroral X-ray images obtained by the imager with 8 NaI(Tl) counters. The darkest parts in the figure are the most bright X-ray source regions. Directions of N_m shows the geomagnetic northward. It is consistent with the X-ray images shown in Fig. 7 that these X-ray images have no simple stable arc structure and bright regions as labeled as A and B drifted slowly with $\sim 50 \, km \, min^{-1}$ roughly to the geomagnetic south-east.

4. Discussion

KREMSER *et al.* (1982) observed the auroral X-rays at different latitudes, using three balloons simultaneously flown in the northern auroral zone. They measured an auroral X-ray enhancement at a substorm onset, with a delay in an abrupt increase of the auroral X-rays at the high latitude. They attributed the delay of the energetic particle precipitation to a poleward movement of precipitation region with $\sim$200 km min^{-1}. However, such poleward movement of the energetic electron precipitation region is often observed at the substorm onset in high latitudes of L=6–7. MAUK *et al.* (1981) observed a small scale ($\sim$15 km) spatial structure of auroral X-rays, but orientation of the image maps were unknown and the time presolution was 10 s. GOLDBERG *et al.* (1982) observed fine auroral X-ray images by a rocket-borne instrument. They were localized X-ray enhancements with a small scale size of 10–30 km in the nighttime ($\sim$0027 MLT) event. However, these results were due to measurements using the sky-scanning method with a NaI(Tl) scintillation counter. IMHOF *et al.* (1985b) observed isolated patches of auroral X-ray emissions at high latitudes. Energies of the auroral X-rays observed there were lower than those in the present experiment. The auroral X-ray images have been hitherto observed mostly by scanning survey methods with a single counter or a one-dimensional array of plural counters. In the present experiment the two-dimensional SSD imager was used.

Gross features of the auroral X-ray images observed by the two X-ray imagers were similar to one another, and they showed unstable brightness varying with time and irregular spatial structure. Comparing the successively observed images, the auroral X-ray source regions seem to drift slowly with an approximate speed of 50 km min^{-1} roughly toward the geomagnetic south-east. As a whole, it is likely that the auroral X-ray images obtained in this event have no typical stable arc structure.

These new imagers enabled us to distinguish the spatial structure of auroral X-rays from its temporal variation with 3 s resolution for the SSD imager. Therefore, the auroral X-ray images obtained in our experiment are realistic. Also another imager of NaI(Tl) counters array confirmed the SSD results. The X-ray event in this flight was measured at a comparatively low latitude (L=5.2), at $\sim$2330 UT ($\sim$2334 MLT) near the magnetic midnight in the expansion phase of a substorm. It is seen from the magnetograms that the present X-ray event was in the expansion phase. This event was in the different phase of the substorm from the event in onset phase analyzed by KREMSER *et al.* (1982). Features of the event observed by us are as the followings. (i) Irregular auroral X-ray images with small scale ($\sim$10 km) spatial structure and dynamic motion were observed. (ii) The localized bright auroral X-ray source regions appeared or disappeared from time to time. (iii) Some parts of the bright regions drifted slowly with a speed of about 50 km min^{-1} toward the geomagnetic south-east. Thus, the these results suggest that localized intermittent precipitations of energetic electrons with several tens keV or greater are possible in the expansion phase of an auroral substorm.

Acknowledgments

References

GOLDBERG, R. A., BARCUS, J. R. and TREINISH, L. A. (1982): Mapping of auroral X-rays from rocket overflights. J. Geophys. Res., **87**, 2509–2524.

HIRASIMA, Y., MURAKAMI, H., OKUDAIRA, K., FUJII, M., NISHIMURA, J., YAMAGAMI, T. and KODAMA, M. (1983): Image-forming detectors to observe fine spatial distributions of auroral X-rays. Mem. Natl Inst. Polar Res., Spec. Issue, **26**, 169–179.

IMHOF, W. L., KILNER, J. R. and REAGAN, J. B. (1985a): Morphological study of energetic electron precipitation events using the satellite bremsstrahlung X ray technique. J. Geophys. Res., **90**, 1543–1552.

IMHOF, W. L., VOSS, H. D., DATLOWE, D. W. and MOBILIA, J. (1985b): Bremsstrahlung X ray images of isolated electron patches at high latitudes. J. Geophys. Res., **90**, 6515–6524.

KODAMA, M. and OGUTI, T. (1976): Spatial distributions of auroral zone X-rays as viewed from rocket altitudes. Mem. Natl Inst. Polar Res., Ser. A (Aeronomy), **14**, 58 p.

KREMSER, G., WILHELM, K., RIEDLER, W., BRØNSTAD, K., TREFALL, H., ULLALAND, S. L., LEGRAND, J. P., KANGAS, J. and TANSKANEN, P. (1973): On the morphology of auroral-zone X-ray events—II. Events during the early morning hours. J. Atmos. Terr. Phys., **35**, 713–733.

KREMSER, G., BJORDAL, J., BLOCK, L. P., BRØNSTAD, K., HÅVÅG, M., IVERSEN, I. B., KANGAS, J., KORTH, A., MADSEN, M. M., NISKANEN, J., RIEDLER, W., STADSNES, J., TANSKANEN, P., TORKAR, K. M. and ULLALAND, S. L. (1982): Coordinated balloon-satellite observations of energetic particles at the onset of a magnetospheric substorm. J. Geophys. Res., **87**, 4445–4453.

MARAL, G., BRØNSTAD, K., TREFALL, H., KREMSER, G., SPECHT, H., TANSKANEN, P., KANGAS, J., RIEDLER, W. and LEGRAND, J. P. (1973): On the morphology of auroral-zone X-ray events—III. Large-scale observation in the midnight-to-morning sector. J. Atmos. Terr. Phys., **36**, 735–751.

MAUK, B. H., CHIN, J. and PARKS, G. (1981): Auroral X-ray images. J. Geophys. Res., **86**, 6827–6835.

NAKAMOTO, A., MURAKAMI, H., OKUDAIRA, K., HIRASIMA, Y., YAMAGAMI, T., OHTA, S., NAMIKI, M., NISHIMURA, J., KODAMA, M., MIYAOKA, H., SATO, N. and FUJII, R. (1985): Mozaikugata Si(Li) handôtai kenshutsuki ni yoru ôrora X-sen satsuzô kansoku keikaku (Project of auroral X-ray image observations using two-dimensional array of Si(Li) semiconductor detectors). Nankyoku Shiryô (Antarct. Rec.), **87**, 32–45.

ULLALAND, S., STADSNES, J., HÅVÅG, M., BJORDAL, J., BRØNSTAD, K., KREMSER, G., KORTH, J., BLOCK, L. P., IVERSEN, I. B., TORKAR, K. M., RIEDLER, W., KANGAS, J., TANSKANEN, P., STAUNING, ·P. and AMATA, E. (1984): Observations during a magnetospheric substorm triggered by an SSC; A case study. Proc. Conf. Achievements of the IMS, 26–28 June 1984, Graz, Austria, 309–314.

Appendix

Relative accuracy of a position of a regular square pixel (side-length is a) is denoted as Δ. Coordinate system as shown in Fig. A-1 is adopted. Square of Δ is mathematically equivalent to "variance." The variance Δ^2 is defined by

$$\Delta^2 = \frac{\int_{-a/2}^{a/2} dx \int_{-a/2}^{a/2} dy\{(x-0)^2+(y-0)^2\}}{a^2}.$$

Although z is a counting rate coordinate, z is defined to be a unity for normalization, when accuracy of the position of the pixel is discussed. As result of integral calculation, $\Delta^2 = a^2/6$, then $\Delta = a/\sqrt{6}$. This means that transverse or longitudinal accuracy of the position is $1/\sqrt{6}$ times of the side-length.
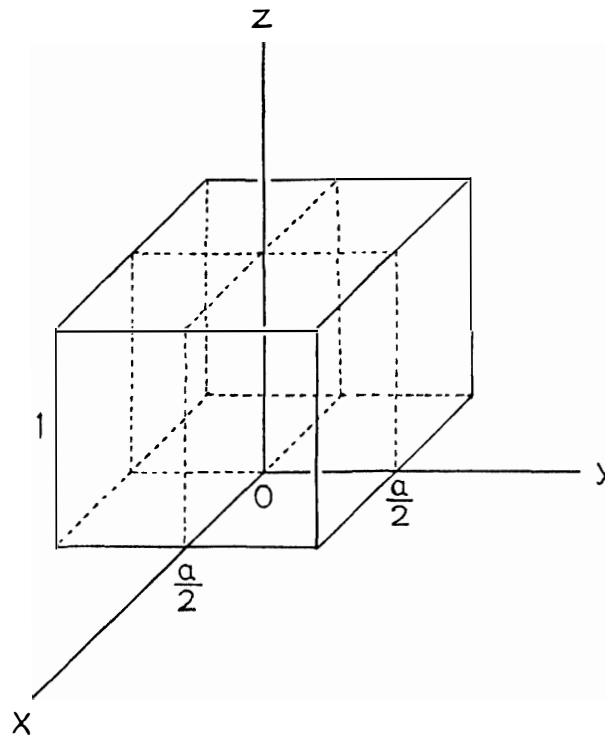
Fig. A-1. Coordinate system of a regular square pixel.